A NOVEL SEQUENTIAL MONTE CARLO FILTER WITH GAUSSIAN MIXTURE MODELS AND KERNEL DENSITY ESTIMATION

Sehyun Yun[*], Renato Zanetti[†] and Brandon A. Jones[‡]

In this paper, a modified kernel-based ensemble Gaussian mixture filtering (EnGMF) is introduced to produce fast and consistent orbit determination capabilities in a sparse measurement environment. The EnGMF is based on kernel density estimation (KDE) to combine particle filters and Gaussian sum filters. This work proposes using Silverman's rule of thumb to reduce the computational burden of KDE. Equinoctial orbital elements are used to improve the accuracy of the KDE bandwidth parameter in the modified EnGMF. Through numerical simulation, the proposed implementation is compared to state-of-the-art approaches in terms of accuracy, consistency, and computational speed.

INTRODUCTION

In recent years, there has been an increasing interest in tracking an ever-growing number of space objects (SOs) for collision avoidance and space domain awareness.[1–3] As very large, low earth orbit (LEO) constellations are being developed and launched, the risk of collision in LEO keeps increasing because of a high density of SOs in this region. The high number and density of LEO SOs require accurate orbit determination and data association.[4] Currently, only a limited number of radar-based surveillance sensors are available and used to estimate the state of an SO in LEO. The current approach to maintaining a LEO catalogue is not scalable to tens of thousands of spacecrafts. The solution of this problem is either adding more hardware (more tracking stations and/or clusters of supercomputers) or improving the computational efficiency of tracking and data association software used to maintain the catalogue.

A software-only solution is one in which the number of available measurements per SO is reduced because the current surveillance network is tasked to acquire data from many more SOs. It requires an efficient data association algorithm and an estimator able to extract as much information as possible from the sparse data. This paper addresses the latter, and proposes an accurate and computationally fast nonlinear estimation algorithm for orbit determination.

For linear systems with linear measurements, the well-known Kalman filter[5] provides a globally optimal solution, i.e., it extracts as much information from the data as possible (in a minimum mean square error sense). In the presence of nonlinearities (either in the dynamics, the measurements, or both), a nonlinear filter is able to produce a more accurate estimate than a linear one, i.e., extract more information from the data. Radar measurements of range, range-rate, and angles to an SO are inherently nonlinear. A nonlinear filter, therefore, will outperform a linear filter such as the extended Kalman filter (EKF)[6] or unscented Kalman filter (UKF)[7] even in the presence of near-linear dynamics.

[*]Ph.D. Candidate, Department of Aerospace Engineering and Engineering Mechanics, The University of Texas at Austin, Austin, TX 78712.

[†]Assistant Professor, Department of Aerospace Engineering and Engineering Mechanics, The University of Texas at Austin, Austin, TX 78712.

[‡]Assistant Professor, Department of Aerospace Engineering and Engineering Mechanics, The University of Texas at Austin, Austin, TX 78712.

To cope with the sparse data problem, this paper compares two nonlinear algorithms: the adaptive entropy-based Gaussian mixture information synthesis (AEGIS)[8] and the kernel-based ensemble Gaussian mixture filtering (EnGMF).[9] This work proposes a new modification to EnGMF to greatly improve its computational complexity. Two implementations of the UKF are also compared to the proposed approach, representing the SO with both Cartesian and equinoctial coordinates.[10]

For linear measurements and dynamics, the UKF reduces to the Kalman filter and is the optimal output of all linear estimators regardless of the probability distributions (in a minimum mean square error, MMSE, sense). The UKF is typically more robust to nonlinearities than the EKF[7] but can still fail to produce an adequate estimate in the case of high nonlinearities. The nonlinearities of orbital dynamics are easily mitigated by choosing to represent the SO's state with an appropriate set of orbital elements, for example equinoctial elements. Changes in these elements, specifically the angle quantity, are linear, and variations due to nonlinear effects are relatively small. This choice of coordinates, therefore, allows for accurate and computationally inexpensive long time propagations of the mean and covariance matrix,[11,12] for example when using the unscented transformation (UT). The price to pay for linear dynamics is typically an even more nonlinear measurement model, which may cause UKF divergence in a scarce-measurement environment, as shown in the numerical results section of this paper. In measurement-rich environments, when long propagations are followed by dense measurements arcs, a batch least-squares approach is often the preferred orbit determination solution,[13] as it allows to extract more information from nonlinear measurements than linear sequential filters. After processing the measurement batch, the mean and covariance of the estimate can be propagated with the UT to start a new iteration. Batch least squares does not provide full information about the probability distribution function and it only returns the mean and covariance matrix and the underlying distribution is typically assumed Gaussian, hence they work best when many measurements are available such that the resulting uncertainty is close to Gaussian. Nonlinear recursive filters, on the other hand, approximate the optimal MMSE estimator, which has the lowest square estimation error (on average), and provides a full description of the underlying PDFs. AEGIS and our proposed modification to EnGMF are two examples of nonlinear filters.

While this work focuses on the estimation problem, adding data association to a single-target nonlinear filter is a well-studied problem. Data association and collision detection benefit from full knowledge of the PDF, which can be approximated with AEGIS and the EnGMF but inevitably results in a Gaussian assumption for linear estimators. As long as the PDF remains approximately Gaussian after measurements are incorporated, linear filters produce excellent performance. Ref.,[14] for example, assumes that the initial orbit determination solution is an estimate with a Gaussian distribution, and employs modified equinoctial elements to propagate the state and associate a sequence of observations to an SO using the Mahalanobis distance.

The AEGIS method is based on the standard Gaussian sum filter (GSF).[15,16] The GSF is a nonlinear estimator for nonlinear systems and it has been applied to SO tracking applications.[17,18] To deal with multimodal and non-Gaussian distributions, the GSF approximates the probability density functions (PDF) as a Gaussian mixture model (GMM). The GSF provides a nearly optimal solution when enough components are taken and each Gaussian component has a small enough covariance matrix such that the nonlinear dynamic and measurement functions can be accurately approximated to linear functions in the support of each Gaussian component. In the presence of a Gaussian prior and a nonlinear measurement, the GSF outperforms linear filters when the prior is approximated by many Gaussian of smaller covariance such that the measurement is approximately linear in their support.

One of the limitations of the standard GSF is that the weights of the Gaussian components remain the same during nonlinear propagations. Several studies recently have been proposed to address this issue and improve the standard GSF algorithm to better account for nonlinear dynamics.[8,19,20] One of these

approaches is AEGIS, which splits the Gaussian components to reduce the effects of nonlinearities of a dynamical system during the prediction of state uncertainty.[8]

Another approach to nonlinear filtering is sequential importance sampling with resampling (SISR), commonly known as particle filters (PFs).[21] PFs are known to suffer from degeneracy with near-deterministic dynamics, i.e., with little process noise. As orbital dynamics is well characterized, a particle filter implementation of orbit determination inevitably requires low process noise. Modifications have been investigated to improve the standard SISR methods such as the bootstrap particle filter (BPF), auxiliary particle filter (APF), and regularized particle filter (RPF)[22] by combining particle filters and GSF.[9,23–26] For example, the sequential Monte Carlo filtering with Gaussian mixture model (SMCGMM) proposed in[23] assumes that each particle of the pre-propagation distribution to be a Gaussian component having a zero or small covariance matrix. Refs.[24] and[25] integrate a PF with a clustering algorithm (e.g., K-means algorithm or expectation-maximization (EM) algorithm) to approximate the prior distribution with a GMM. Although clustering to form the GMM provides an accurate solution for a highly nonlinear system, it is computationally expensive and not of practical use for tracking large LEO constellations.

Other examples of hybrid PF/GSF algorithms include Refs.[9] and[26] which approximate each propagated particle as a Gaussian component with a non-zero covariance matrix calculated by bandwidth selection for kernel density estimation (KDE). KDE is a non-parametric technique to estimate the PDF of a random variable.[27] The KDE algorithm with a Gaussian kernel is similar to the EM clustering algorithm in that they construct a GMM using the particles. However, in the KDE algorithm, every particle is considered as a Gaussian component to establish a GMM whereas EM clustering algorithm groups several particles into each Gaussian mixture components. An adaptable bandwidth selection suffers from a high computational cost similar to the clustering algorithms presented in[24] and.[25]

In this paper, the EnGMF algorithm is modified to efficiently track SOs in LEO with short and sparse observation data. A key element of the EnGMF algorithm is the determination of the covariance matrix of each Gaussian component in a GMM. The covariance matrix is determined by the bandwidth parameter of a kernel function. Although the optimal bandwidth parameter can be obtained using a data-driven method,[28,29] this approach is computationally expensive. Alternatively, we can compare the simulation results of a system using a range of the bandwidth parameter[26] and tune this parameter according to the system. In this paper, we propose an approach to achieve a near-optimal bandwidth parameter with a low computational cost for orbit determination with sparse observation data. We achieve this by computing the bandwidth of a Gaussian kernel in the KDE algorithm with Silverman's rule of thumb[30] to reduce the KDE computational burden.

The remainder of this paper is organized as follows. First, the dynamics and measurement models are described and the coordinate systems are presented. Then, the two nonlinear estimation techniques, the AEGIS and a modified EnGMF, are introduced in section III. In section IV, simulation results are shown using the proposed algorithms followed by some concluding remarks on the methodology and results.

SYSTEM MODELS

Dynamics Model

The inertial position and velocity of an SO are denoted by $\boldsymbol{r}^I = [x\ y\ z]^{\mathrm{T}}$ and $\boldsymbol{v}^I = [v_x\ v_y\ v_z]^{\mathrm{T}}$. The orbital dynamics of an SO in Earth-Centered Inertial (ECI) coordinates are given by

$$\begin{bmatrix} \dot{\boldsymbol{r}}^I \\ \dot{\boldsymbol{v}}^I \end{bmatrix} = \begin{bmatrix} \boldsymbol{v}^I \\ -\frac{\mu}{r^3}\boldsymbol{r}^I + \boldsymbol{a}^I_{NS} + \boldsymbol{a}^I_{3B} + \boldsymbol{a}^I_{drag} + \boldsymbol{a}^I_{srp} \end{bmatrix} \tag{1}$$

where μ is the Earth's gravitational parameter and r is the Euclidean norm of $\boldsymbol{r}^I$. $\boldsymbol{a}^I_{NS}$ is the gravitational perturbation due to non-spherical effect of the Earth gravity, $\boldsymbol{a}^I_{3B}$ indicates the third-body perturbations of

the Moon and the Sun, and $\boldsymbol{a}^I_{drag}$ and $\boldsymbol{a}^I_{srp}$ represent the acceleration perturbation due to atmospheric drag and solar radiation pressure (SRP), respectively. For this study, the EGM2008[31] gravity model is used for the Earth and 70 $\times$ 70 degrees and order are applied for gravity modeling, and the planetary and lunar ephemeris DE430[32] is selected to compute the location of the Moon and the Sun.

The primary non-gravitational force acting on SOs in low earth orbit (LEO) is the drag force. The drag acceleration due to atmospheric density relies upon the drag coefficient, the cross-sectional area of an SO face perpendicular to velocity vector, and the height of an SO above the Earth's surface. The acceleration due to drag is then given by

$$\boldsymbol{a}^I_{drag} = -\frac{1}{2} C_d \frac{A}{m} \rho_d \|\boldsymbol{v}_{rel}\| \boldsymbol{v}_{rel} \tag{2}$$

where C_d is the drag coefficient, m and A are the mass and cross-sectional area of the SO, respectively, ρ_d is the atmospheric density at altitude of the SO, $\|\cdot\|$ means the Euclidean norm, and $\boldsymbol{v}_{rel}$ is the atmosphere-relative velocity vector. For computing the atmospheric density, the exponential density model is employed in this study.[33]

The acceleration due to SRP depends on the shape of an SO and the cannonball model, i.e., spherical object, is assumed in this paper. The acceleration perturbation due to SRP is then given by

$$\boldsymbol{a}^I_{srp} = -\frac{S_F A C_R \boldsymbol{u}^I_{sun}}{mc} \tag{3}$$

where S_F is the solar flux, m is the mass of the SO, c is the speed of light, C_R is the coefficient of reflectivity, u^I_{sun} is the unit vector pointing from the SO to the Sun in the ECI frame.

Measurement Model

Range ρ_{range} and range-rate $\rho_{rangerate}$ measurements along the line of sight (LOS) from a ground-based radar sensor to an SO is provided. The relative position vector $\boldsymbol{\rho}^I = [\rho_x \ \rho_y \ \rho_z]^{\mathrm{T}}$ between the SO and a ground station $\boldsymbol{r}^I_S$ coordinatized in ECI is given by:

$$\boldsymbol{\rho}^I = \boldsymbol{r}^I - \boldsymbol{r}^I_S \tag{4}$$

The error-free range measurement is given:

$$\rho_{range} = \|\boldsymbol{\rho}^I\| = \|\boldsymbol{r}^I - \boldsymbol{r}^I_S\| \tag{5}$$

By differentiating Eq. (5) with respect to time, the error-free range-rate measurement is obtained as follows:

$$\rho_{rangerate} = \frac{\left(\boldsymbol{r}^I - \boldsymbol{r}^I_S\right)^{\mathrm{T}} \left(\boldsymbol{v}^I - \boldsymbol{v}^I_S\right)}{\|\boldsymbol{r}^I - \boldsymbol{r}^I_S\|} \tag{6}$$

where $\boldsymbol{v}^I_S$ is the time rate of change of the ground station position vector with respect to the inertial frame.

Along with the range and range-rate, angle data in the form of right ascension α and declination δ are measured to estimate the states of the SO. The error-free angle observation equations are described as follows:

$$\alpha = \tan^{-1}\left(\frac{\rho_y}{\rho_x}\right), \quad \delta = \sin^{-1}\left(\frac{\rho_z}{\|\boldsymbol{\rho}^I\|}\right) \tag{7}$$

All measurements are corrupted by zero-mean, Gaussian noise. In this study, light travel time delay and measurement biases are not considered.

Coordinate systems

The dynamic equations of the SO presented above are expressed in Cartesian coordinates, which results in nonlinear differential equations. Alternatively, equinoctial orbital elements[10] offer a near-linear dynamics. The Keplerian motion is exactly linear, and nonlinearities arise only due to perturbations such as non-central gravity and drag. The equinoctial orbital elements are expressed as functions of the Keplerian orbital elements as follows:

$$\begin{aligned} a &= a \\ h &= e \sin(\omega + \Omega) \\ k &= e \cos(\omega + \Omega) \\ \lambda_0 &= M_0 + \omega + \Omega \\ p &= \tan(i/2) \sin(\Omega) \\ q &= \tan(i/2) \cos(\Omega) \end{aligned} \tag{8}$$

where a is the semi-major axis, e is the eccentricity, i is the inclination, Ω is the longitude of the ascending node, ω is the argument of periapsis, and M_0 is the mean anomaly.

ESTIMATION TECHNIQUES

This section reviews the UKF and AEGIS and introduces the proposed nonlinear estimation algorithms to cope with the sparse data problem: a modified EnGMF.

Unscented Kalman Filter

The UKF approximates nonlinear functions with statistical linearization using a set of sigma points.[34] The most common schemes to effectively calculate sigma points are to assume that all distributions are Gaussian.[7] Given an $n_{\boldsymbol{x}} \times n_{\boldsymbol{x}}$ error covariance matrix $P^{xx}_{k|k}$, we generate $2n_{\boldsymbol{x}} + 1$ sigma points as follows:

$$\mathcal{X}_{k|k} = \hat{\boldsymbol{x}}_{k|k} \mathbb{1}_{1\times(2n_{\boldsymbol{x}}+1)} + \left[\mathbf{0}_{n_{\boldsymbol{x}}\times 1},\ \sqrt{n_{\boldsymbol{x}} + \lambda} S_k\right] \tag{9}$$

where $n_{\boldsymbol{x}}$ is the dimension of the state, k is an integer that indicates the discrete time step, $\hat{\boldsymbol{x}}_{k|k}$ is the a posteriori state estimate, $\mathbb{1}_{1\times(2n_{\boldsymbol{x}}+1)}$ is an indicator function,

$$S_k = \left[\left(P^{xx}_{k|k}\right)^{1/2} - \left(P^{xx}_{k|k}\right)^{1/2}\right], \tag{10}$$

$\left(P^{xx}_{k|k}\right)^{1/2}$ is the square root of the $P^{xx}_{k|k}$ such that $P^{xx}_{k|k} = \left(P^{xx}_{k|k}\right)^{1/2}\left(P^{xx}_{k|k}\right)^{1/2(\mathrm{T})}$, and $\lambda = \alpha^2(n_{\boldsymbol{x}}+\kappa) - n_{\boldsymbol{x}}$ is a scaling parameter.[35] The parameter α tunes the spread of the sigma points around $\hat{\boldsymbol{x}}_{k|k}$ and it is usually set to a small positive number ($10^{-4} \leq \alpha \leq 1$). κ is a secondary scaling parameter which is usually set to $3 - n_{\boldsymbol{x}}$. Based on the above sigma points, the corresponding weights are calculated as follows:

$$W^m_0 = \frac{\kappa}{n_{\boldsymbol{x}} + \kappa}, \quad W^c_0 = \frac{\kappa}{n_{\boldsymbol{x}} + \kappa} + (1 - \alpha^2 + \beta) \tag{11}$$

$$W^m_j = W^c_j = \frac{0.5}{n_{\boldsymbol{x}} + \kappa}, \quad \text{for } j = 1, \cdots, 2n_{\boldsymbol{x}} \tag{12}$$

where the parameter β is used to include prior knowledge of the distribution of $\boldsymbol{x}$. With the above sigma points and weights, the time update equations are expressed as follows:

$$\mathcal{X}_{j,k+1|k} = \boldsymbol{f}_k(\mathcal{X}_{j,k|k}), \quad j = 0, \cdots, 2n_{\boldsymbol{x}} \tag{13}$$

$$\hat{\boldsymbol{x}}_{k+1|k} = \sum_{j=0}^{2n_{\boldsymbol{x}}} W_j^m \mathcal{X}_{j,k+1|k} \tag{14}$$

$$P_{k+1|k}^{xx} = \sum_{j=0}^{2n_{\boldsymbol{x}}} W_j^c \left[\mathcal{X}_{j,k+1|k} - \hat{\boldsymbol{x}}_{k+1|k}\right] \left[\mathcal{X}_{j,k+1|k} - \hat{\boldsymbol{x}}_{k+1|k}\right]^{\mathrm{T}} + Q_k \tag{15}$$

where $\boldsymbol{f}_k$ is the nonlinear dynamic function, $\hat{\boldsymbol{x}}_{k+1|k}$ is the a priori state estimate, $P_{k+1|k}^{xx}$ is the a priori state estimation error covariance, and Q_k is the covariance matrix of the process noise ν_k. It is assumed that ν_k is independent from the initial distribution of $\boldsymbol{x}$. Using the propagated estimates $\hat{\boldsymbol{x}}_{k+1|k}$ and $P_{k+1|k}^{xx}$, a new set of sigma points $\mathcal{X}_{k+1|k}$ and the corresponding weights are recalculated. The measurement update equations are then expressed as follows:

$$\mathcal{Y}_{j,k+1|k} = \boldsymbol{h}_{k+1}(\mathcal{X}_{j,k+1|k}), \quad j = 0, \cdots, 2n_{\boldsymbol{x}} \tag{16}$$

$$\hat{\boldsymbol{y}}_{k+1} = \sum_{j=0}^{2n_{\boldsymbol{x}}} W_j^m \mathcal{Y}_{j,k+1|k} \tag{17}$$

$$P_{k+1|k}^{yy} = \sum_{j=0}^{2n_{\boldsymbol{x}}} W_j^c \left[\mathcal{Y}_{j,k+1|k} - \hat{\boldsymbol{y}}_{k+1}\right] \left[\mathcal{Y}_{j,k+1|k} - \hat{\boldsymbol{y}}_{k+1}\right]^{\mathrm{T}} + \boldsymbol{R}_{k+1} \tag{18}$$

$$P_{k+1|k}^{xy} = \sum_{j=0}^{2n_{\boldsymbol{x}}} W_j^c \left[\mathcal{X}_{j,k+1|k} - \hat{\boldsymbol{x}}_{k+1|k}\right] \left[\mathcal{Y}_{j,k+1|k} - \hat{\boldsymbol{y}}_{k+1}\right]^{\mathrm{T}} \tag{19}$$

$$\hat{\boldsymbol{x}}_{k+1|k+1} = \hat{\boldsymbol{x}}_{k+1|k} + P_{k+1|k}^{xy} \left(P_{k+1|k}^{yy}\right)^{-1} \left(\boldsymbol{y}_{k+1} - \hat{\boldsymbol{y}}_{k+1}\right) \tag{20}$$

$$P_{k+1|k+1}^{xx} = P_{k+1|k}^{xx} - P_{k+1|k}^{xy} \left(P_{k+1|k}^{yy}\right)^{-1} \left(P_{k+1|k}^{xy}\right)^{\mathrm{T}} \tag{21}$$

where $\boldsymbol{h}_{k+1}$ is the nonlinear measurement function, $P_{k+1|k}^{yy}$ is the measurement residual covariance, $P_{k+1|k}^{xy}$ is the cross covariance, and $\boldsymbol{R}_{k+1}$ is the covariance matrix of the measurement noise $\boldsymbol{\eta}_{k+1}$. $\boldsymbol{\eta}_{k+1}$ is assumed to be independent from all other random quantities.

Adaptive Entropy-based Gaussian Mixture Information Synthesis

AEGIS uses an entropy-based method to detect nonlinearity of a dynamical system during the prediction of state uncertainty and then applies a splitting technique to decrease the approximation error caused by truncating the nonlinear functions of the system to low-order. The AEGIS method is based on the standard GSF which is a nonlinear estimator. In the GSF, non-Gaussian PDFs are approximated as a GMM as follows:

$$p(\boldsymbol{x}) = \sum_{i=1}^{N} \omega^{(i)} n(\boldsymbol{x}; \boldsymbol{\mu}^{(i)}, P^{(i)}) \tag{22}$$

where $\boldsymbol{x}$ is a random variable, $p(\boldsymbol{x})$ is the PDF of $\boldsymbol{x}$, N is the number of all Gaussian components, $n(\boldsymbol{x}|\boldsymbol{\mu}, P)$ represents the Gaussian PDF with mean $\boldsymbol{\mu}$ and covariance P; and $\boldsymbol{\mu}^{(i)}$, $P^{(i)}$, and $\omega^{(i)}$ are the means, covariance matrices, and weights of the i^{th} Gaussian component. The PDF normalization and positivity properties

lead to the following constraints on the weights:

$$\omega^{(i)} \geq 0, \ \forall i \qquad \sum_{i=1}^{N} \omega^{(i)} = 1 \tag{23}$$

The performance of the GSF mainly depends on both the number and the weights of the components of a GMM; however, both of them are held constant during the propagation step. To improve the standard GSF algorithm to better adapt to nonlinearities of the system, the AEGIS approach allows for the modification of the Gaussian components over the propagation step based on two main mechanisms.

The first step of AEGIS is to monitor the nonlinearity of the dynamics using a property derived from the differential entropy for linearized dynamical systems. The differential entropy of a continuous random variable $\boldsymbol{x}$ is defined as follows:[8]

$$H(\boldsymbol{x}) = -\int_S p(\boldsymbol{x}) \log\left(p(\boldsymbol{x})\right) d\boldsymbol{x} = E\{-\log\left(p(\boldsymbol{x})\right)\} \tag{24}$$

where S is the support set. In this paper, all logarithms are assumed to be natural. The analytic solution of the differential entropy for a multivariate Gaussian distribution is then expressed as follows:

$$H(\boldsymbol{x}) = \frac{1}{2} \log |2\pi e P| \tag{25}$$

where P is the covariance matrix and $|\cdot|$ represents the matrix determinant. By taking a derivative with respect to time for Eq. (25), the time rate of the differential entropy can be calculated as follows:

$$\dot{H}(\boldsymbol{x}) = \frac{1}{2} \text{trace}\{P^{-1}\dot{P}\} \tag{26}$$

where $\dot{P}$ is the time rate of change of the covariance matrix, which in the absence of process noise evolves as:

$$\dot{P}(t) = F\left(\boldsymbol{\mu}(t), t\right) P^{\mathrm{T}}(t) + P(t) F^{\mathrm{T}}\left(\boldsymbol{\mu}(t), t\right) \tag{27}$$

where $\boldsymbol{\mu}(t)$ is the time-varying mean of the Gaussian distribution and $F\left(\boldsymbol{\mu}(t), t\right)$ is the Jacobian of the dynamics evaluated at the mean $\boldsymbol{\mu}(t)$. By substituting Eq. (27) into Eq. (26), the time rate of the differential entropy for a linearized dynamical system is obtained as follows:

$$\dot{H}(\boldsymbol{x}) = \text{trace}\{F\left(\boldsymbol{\mu}(t), t\right)\} \tag{28}$$

Therefore, the entropy value for a linearized system can be calculated by numerically integrating Eq. (28) with an appropriate initial condition, which requires only the evaluation of the trace of the dynamics Jacobian. On the other hand, a nonlinear determination of the differential entropy can be evaluated via Eq. (25) by a nonlinear implementation of the integration of the covariance matrix; for example, unscented transformation is one of the most popular and effective methods for moment evaluation. Any deviation between the linear and nonlinear values of the entropy then indicates that nonlinearity is impacting the Gaussian component. As a result, the difference between the linearized and nonlinear predictions of the entropy can be monitored without the full solution to both the linearized and nonlinear predictors. In other words, when the difference between these values of entropy exceeds a preassigned threshold, a splitting algorithm is applied to the Gaussian component during a propagation. A smaller threshold leads to more frequent splitting during the propagation.

Once the nonlinear effects have been detected from the first step, a splitting algorithm is applied to mitigate the effects by replacing a Gaussian component with several Gaussian components. For the univariate

Table 1. Three-component splitting library

i	ω_i	μ_i	σ_i
1	0.2252246249	-1.0575154615	0.6715662887
2	0.5495507502	0	0.6715662887
3	0.2252246249	1.0575154615	0.6715662887

case, each Gaussian component can be decomposed into 3 components using splitting libraries which are shown in Table 1. The splitting technique for a univariate case with splitting library can be then extended to the multivariate case by considering the principal directions of the covariance matrix. The details of the algorithm are explained in Ref.[8] After the propagation, the posteriori mean and covariance matrix, and mixture weights are obtained using the measurement update of the standard GSF.

When allowing the number of Gaussian components to grow unbounded, AEGIS is an accurate and consistent estimator. In this work we are interested not only in estimation accuracy, but also in computational efficiency to maintain custody of a very large number of SOs. The proposed solution to achieve this balance of performance versus accuracy is introduced next.

Modified Kernel-Based Ensemble Gaussian Mixture Filtering

As a recursive algorithm, the knowledge of the distribution $p(\boldsymbol{x}_{k-1}|\boldsymbol{y}_{k-1})$ at the prior time is assumed and approximated by N independent and identically distributed (i.i.d.) samples $\boldsymbol{x}_{k-1}^{(i)}$ such that

$$p(\boldsymbol{x}_{k-1}|\boldsymbol{y}_{k-1}) \approx \sum_{i=1}^{N} \frac{1}{N} \delta(\boldsymbol{x}_{k-1} - \boldsymbol{x}_{k-1}^{(i)}) \tag{29}$$

where $\boldsymbol{y}$ is a measurement vector and $\delta(\cdot)$ is the Dirac delta function. Following the same procedure as the BPF,[36] a set of samples at the next time step is obtained using the Markov transition kernel $p(\boldsymbol{x}_k|\boldsymbol{x}_{k-1})$. The Markov kernel indicates the dynamics of a system and all estimators use the true dynamic model without process noise in this paper.

The next step is to convert the samples into Gaussian mixtures using KDE. In other words, each particle is considered as a Gaussian component with non-zero covariance. The approximated GMM of the propagated samples is then expressed as follows:

$$p(\boldsymbol{x}_k) \approx \sum_{i=1}^{N} \frac{1}{N} n(\boldsymbol{x}_k; \boldsymbol{x}_{k|k-1}^{(i)}, B) \tag{30}$$

where the bandwidth matrix B is can be calculated by[26]

$$B = \beta \hat{P} \tag{31}$$

where β is the bandwidth parameter, $0 \leq \beta \leq 1$, and $\hat{P}$ is the sample covariance matrix calculated from the particles. The Gaussian components' means are the particles $\boldsymbol{x}_{k|k-1}^{(i)}$ and all GMM weights are equal to $1/N$. The covariance matrix of each Gaussian component is determined by the bandwidth parameter. The larger bandwidth parameter β, the smaller the probability assigned to the particle and vice versa.

Finally, we can incorporate the measurement information by updating the means, covariance matrices, and the weights of all N Gaussian components in the same way as the measurement update of the GSF. N i.i.d. samples are then drawn from the GMM approximation of the posterior distribution. These samples

are used as a starting point for the next iteration. The details of the measurement update of the GSF and the method to draw N i.i.d. samples from a GMM are explained in.[23]

In the EnGMF algorithm, it is crucial to choose the most appropriate bandwidth which determines the performance of the filter. Bandwith selection is an accuracy vs. computational cost trade off, with the most accurate algorithms numerically solving an optimization problem. In this paper, we propose to use Silverman's rule of thumb[30] to estimate the bandwidth (i.e., covariance) matrix B_S as follows:

$$B_S = \beta_S \hat{P} = \left(\frac{4}{n_{\boldsymbol{x}} + 2} \right)^{\frac{2}{n_{\boldsymbol{x}}+4}} N^{-\frac{2}{n_{\boldsymbol{x}}+4}} \hat{P} \tag{32}$$

We can, therefore, obtain a near-optimal bandwidth parameter for orbit determination with sparse observation data without the need of performing any numerical optimization. If the sampling distribution were Gaussian, Silverman's rule of thumb would provide the optimal bandwidth parameter based on the mean integrated square error (MISE) as a performance criterion.[30] However, it may result in conservative (large) estimates when the distribution is not close to Gaussian. This is a very desirable feature, since inaccuracies results in conservatism rather than over-confidence and divergence. The flow chart of the modified EnGMF for orbit determination is described in Figure 1.

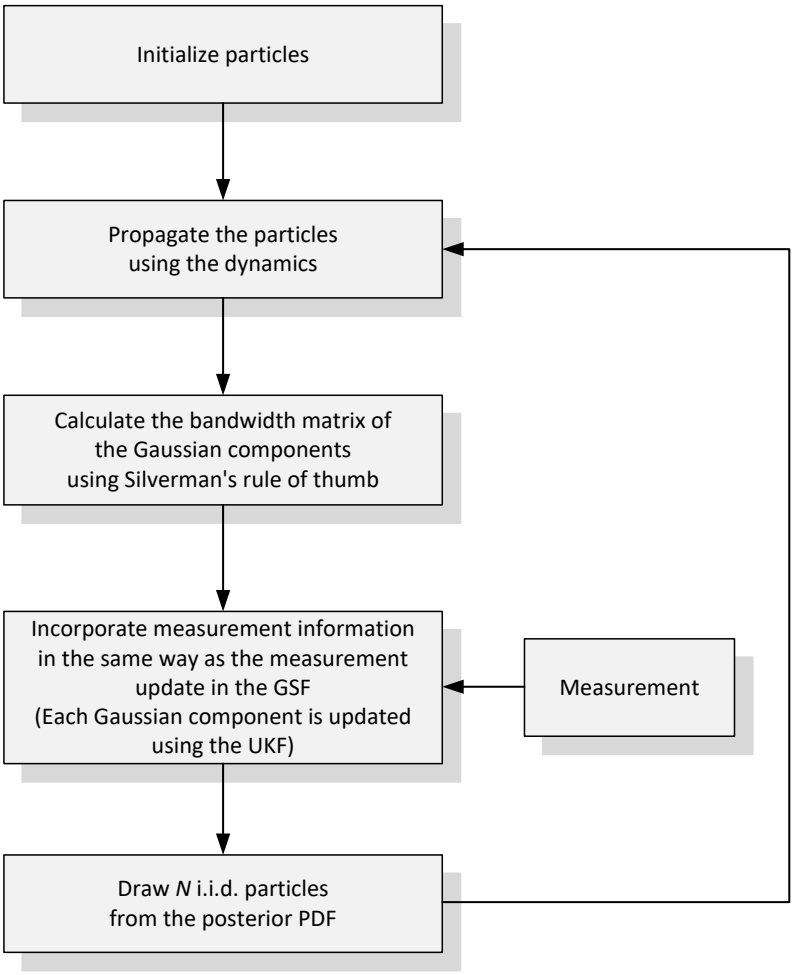

Figure 1. The flow chart of the modified EnGMF for orbit determination

NUMERICAL RESULTS

To evaluate the performance of the UKF, AEGIS, and EnGMF, one numerical example is considered. The system dynamic equations are numerically integrated with an embedded Runge-Kutta 8(7) method.[37] Range, range-rate, and angle measurements are simulated using a ground station located at the North Pole (latitude = 90°, longitude = 0°, altitude = 0 km). In this simulation, observation data are short and sparse, which means that the observation interval time is much longer than the observation duration. The measurements are available every 10 seconds with a pass lasting only 2 minutes, i.e., 12 measurements per pass. Each observation consists of range, range-rate, right ascension, and declination and the measurements are corrupted by additive zero-mean Gaussian white noise with standard deviation of 30 m and 0.3 m/s for the range and range-rate, respectively, and 100 arc-seconds on the right ascension and declination observation.

The SO is in a near polar orbit with the following Keplerian orbital elements: a = 7,078.0068 km, e = 0.01, i = 85°, and $\omega = \Omega = \nu = 0$. The simulation epoch is 4-January-2010 at 00:00:00 UTC. The shape of the SO is assumed to be a sphere with a cross-sectional area of 1 m^2 and a mass of 500 kg. The drag coefficient and the coefficient of reflectivity of the SO are set to be 2 and 1.5, respectively. The initial distribution is defined in Cartesian coordinates as

$$\boldsymbol{x}_0 \sim n\left(\boldsymbol{x}_0;\ \boldsymbol{\mu}_0,\ P_0\right) \tag{33}$$

where

$$\boldsymbol{\mu}_0 = \begin{bmatrix} 7007.2175 \\ 0 \\ 0 \\ 0 \\ 0.6606 \\ 7.5509 \end{bmatrix} \tag{34}$$

$$P_0 = \begin{bmatrix} 1.481e\text{+}2 & 0 & 0 & 0 & -9.237e\text{-}2 & -5.333e\text{-}2 \\ 0 & 2.885e\text{+}1 & 9.994 & -3.232e\text{-}2 & 0 & 0 \\ 0 & 9.994 & 5.770 & -1.242e\text{-}2 & 0 & 0 \\ 0 & -3.232e\text{-}2 & -1.242e\text{-}2 & 3.687e\text{-}5 & 0 & 0 \\ -9.237e\text{-}2 & 0 & 0 & 0 & 6.798e\text{-}5 & 3.145e\text{-}5 \\ -5.333e\text{-}2 & 0 & 0 & 0 & 3.145e\text{-}5 & 3.166e\text{-}5 \end{bmatrix} \tag{35}$$

First, a Monte Carlo analysis is performed with 100 simulations, and each simulation has one measurement pass every orbital period, 5926 seconds. Note that, throughout this paper, the starting time of each measurement pass is randomly selected in close proximity of a multiple of the orbital period. The UKF uses the following tuning parameters: α = 1, β = 2, κ = 3 - d = -3, for its sigma points spread. For the AEGIS method, the three-component splitting library is used (AEGIS-3), and the threshold on the allowed deviation of the differential entropy is set as $\Delta H = 0.001 H_0$.[8] The value of H_0 is unique for each mixture component and based on the covariance at the latter of the last posterior estimate or the output of a splitting operation. After each measurements pass, the AEGIS algorithm is forced to have only one Gaussian component with the posterior mean and covariance matrix. This simple merging algorithm reduces AEGIS computational burden and adds conservatism that cannot cause divergence (a Gaussian distribution is the most uncertain given any finite covariance matrix). The EnGMF method uses 1000 particles. Both the AEGIS and the EnGMF use the UKF measurement update equations for incorporating measurement information in each GMM component. For the UKF and EnGMF, two implementations with Cartesian coordinates and the equinoctial orbital elements are compared. AEGIS is only implemented in Cartesian coordinates. An AEGIS implementation in equinoctial coordinates will result in very few component splits as the splits occur due to nonlinearity in the propagation, making equinoctial AEGIS very similar to the equinoctial UKF.

These three algorithms are compared based on accuracy, complexity, and consistency. The accuracy of the filters is represented by their root-mean-square error (RMSE), which is computed from the true and estimated states at each measurement update time for all Monte Carlo simulations. The filters' complexity is represented by their average execution time per filtering run in a C++ implementation on a 3.2 GHz single-core Ubuntu operating system. The filters' consistency is examined using the scaled normalized estimation error squared (SNEES) β^R which is defined as follows:

$$\beta_k^R = \frac{1}{Md} \sum_{j=1}^{M} (\boldsymbol{x}_k^{(j)} - \hat{\boldsymbol{x}}_k^{(j)})^{\mathrm{T}} (\boldsymbol{P}_k^{(j)})^{-1} (\boldsymbol{x}_k^{(j)} - \hat{\boldsymbol{x}}_k^{(j)}) \tag{36}$$

where M is the number of Monte Carlo simulations, $\boldsymbol{x}_k^{(j)}$ are the true states, $\hat{\boldsymbol{x}}_k^{(j)}$ are the estimated states, $\boldsymbol{P}_k^{(j)}$ are the filter's estimated error covariance matrix of the j-th Monte Carlo run at the time step k. The size of the state space $d = 6$ is used to scale the NEES value[38] such that a consistent filter will result in a SNEES of one rather than a NEES of d. If the SNEES value is much greater than 1, it means the estimator is divergent; however, if the value is much smaller than 1, it indicates the estimator is too conservative. When the estimator is consistent, SNEES should be nearly one at all times.

The time history of the RMS position errors of the 100 simulations is depicted in Figure 2 and the position's RMSE values of each filter are listed in Table 2. Due to their nonlinear nature, AEGIS and EnGMF provide better performance than the UKF at the very first measurement update. However, in this measurement-rich environment, equinoctial UKF performs near the top in accuracy, and it is the most consistent at a small fraction of the computational cost of nonlinear filters. From the results, it is also shown that the UKF and EnGMF with equinoctial orbital elements outperforms the corresponding filter with Cartesian coordinates. Nevertheless, the best performance in terms of estimation accuracy is obtained with the AEGIS, closely followed by equinoctial UKF.

Figure 3 shows the SNEES value for 100 Monte Carlo simulations and the average computation time per filtering run for all the filters. In Figure 3(a), the SNEES value of the EnGMF is smaller than 1, which means the EnGMF is too conservative. For the EnGMF, the covariance matrix calculated by Silverman's rule for each Gaussian component is over-smoothed since the density is not truly Gaussian. The value of the AEGIS filter is gradually increased starting from the value 1. For the UKF, it works better when using equinoctial orbital elements than when using Cartesian coordinates. When the UKF uses Cartesian coordinates, it diverges in two out of 100 simulations, which means the estimate error completely exceeded the ± 3 sigma predicted standard deviations of the posterior covariance matrix. As is typical for linear estimators without underweighting,[39] equinoctial UKF is overly optimistic in processing the very first batch of measurements, but due to the measurement-rich scenario, it recovers nicely and achieved very good consistency.

The time-averaged SNEES value to the total samples of 100 cases is listed in Table 2. The average computation time is also presented in Table 2. In terms of computation time, the best performance is obtained

Table 2. Monte Carlo averaged RMSE, SNEES, and computation time for 100 simulations

	Position's RMSE (km)	SNEES	Computation time (sec)
UKF (Cartesian)	0.2212	507.4479	3.36
UKF (Equinoctial)	0.1839	1.2425	3.55
AEGIS-3 (Cartesian)	0.1810	1.5058	460.34
EnGMF (Cartesian)	0.3320	0.4986	189.47
EnGMF (Equinoctial)	0.3284	0.4920	190.49

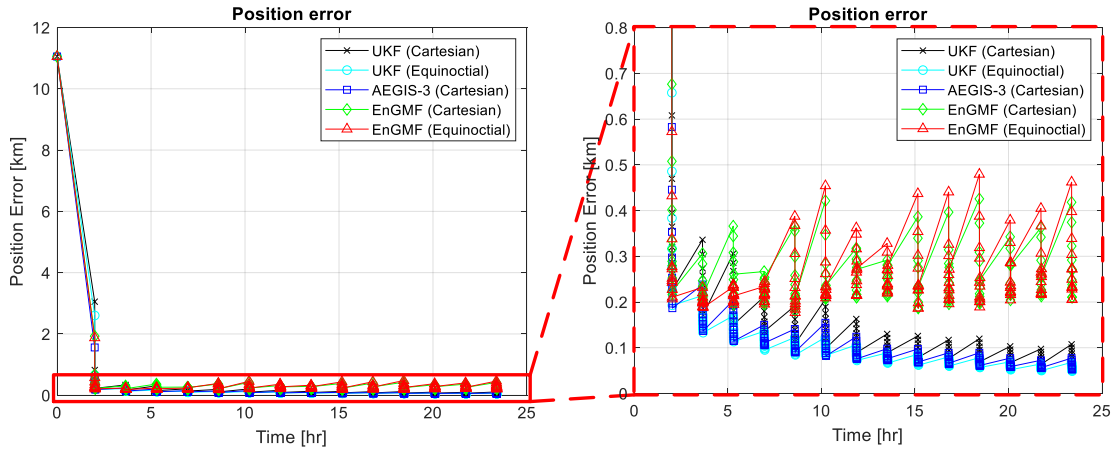

Figure 2. The average RMSE for 100 Monte Carlo simulations, 1 pass per orbit

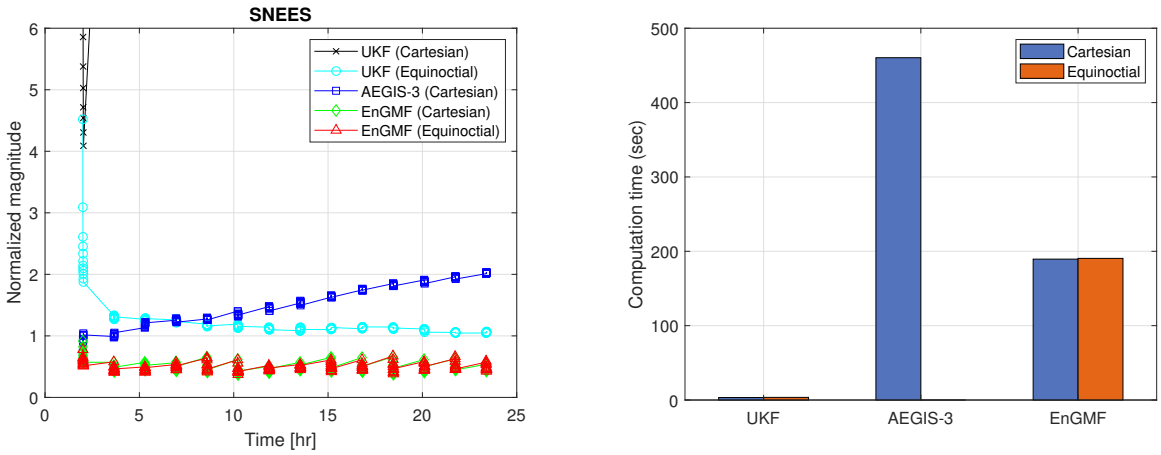

(a) The SNEES value

(b) The average computation time per filtering run

Figure 3. The SNEES value and the average computation time per filtering run for 100 Monte Carlo simulations

with the UKF by a wide margin (as expected from a simple linear filter), and the EnGMF reduces the mean computation time by 58.73% in comparison with the AEGIS. Notice that resetting the GMM in AEGIS to a single component after each measurement pass greatly reduces its computational cost when compared to other merging/pruning schemes.

Having established the baseline performance of the estimators with one measurement pass per orbital period, we focus on the real challenge addressed by this paper: scarcity of measurements. Additional simulations are performed when the gap between measurement passes is increased to 2, 3, 4, 5, and 6 orbital periods. As in the previous case, a Monte Carlo analysis is performed with 100 simulations. As we are concerned with computational speed, we set a maximum allowable number of GMM components for the AEGIS to be 1000 to contain its overall run time, and relaxing this constraint will result in an accurate, but very slow filter.

Figure 4(a) displays the position RMSE of the UKF, AEGIS, and EnGMF in all the six cases and the Monte Carlo averaged RMS position errors for all cases are listed in Table 3, where n/a indicates the filter has diverged. The time-averaged SNEES value of each estimator for all the six cases is displayed in Figure 4(b).

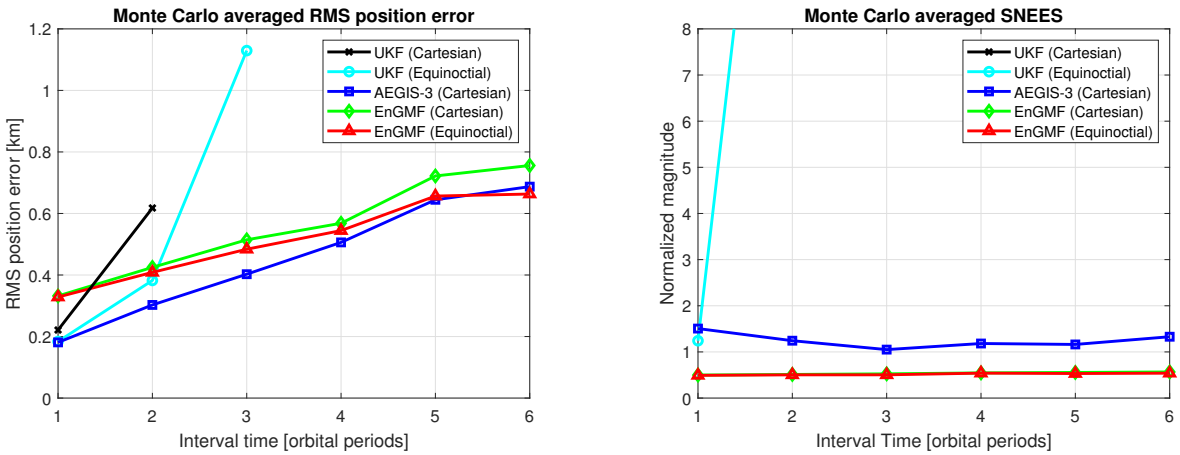

(a) Monte Carlo averaged RMSE

(b) Monte Carlo averaged SNEES value

Figure 4. Monte Carlo averaged RMSE and SNEES value for all the six cases

Table 3. Monte Carlo averaged RMS position errors for all the six cases

	1	2	3	4	5	6
UKF (Cartesian)	0.2212	0.6178	n/a	n/a	n/a	n/a
UKF (Equinoctial)	0.1839	0.3823	1.1294	n/a	n/a	n/a
AEGIS-3 (Cartesian)	0.1810	0.3027	0.4026	0.5060	0.6445	0.6872
EnGMF (Cartesian)	0.3320	0.4248	0.5144	0.5682	0.7219	0.7559
EnGMF (Equinoctial)	0.3284	0.4086	0.4838	0.5444	0.6566	0.6632

The AEGIS outperforms the EnGMF with Cartesian coordinates in terms of RMS accuracy for all the six cases. However, the EnGMF with the equinoctial orbital elements provides better estimation accuracy than the AEGIS when the interval time between measurement passes is 6 orbital periods. Also note that the RMS position error of the AEGIS increases more rapidly with the orbital periods than the EnGMF as shown in Figure 4(a). While the equinoctial UKF provides excellent performance for the one-orbit interval period, its performance is severely degraded in terms of accuracy and consistency for the two- and three-orbits case, and is completely diverging for 4–6 orbital periods in-between measurements pass. This is another confirmation that linear dynamics is not sufficient to justify the use of a linear estimator, as nonlinear measurements also need to be addressed.

The choice of using Silverman's rule in the EnGMF rather than performing bandwidth optimization is a trade between speed and accuracy/consistency. However, since the choice results in a conservative filter (estimated covariance larger than actual one) this trade off is deemed worthy when the goal is to maintain custody of a very high number of SOs. The EnGMF implementation in the equinoctial elements provides better and better performance than the EnGMF with Cartesian coordinates as the interval between measurement passes is increasing. The UKF with Cartesian coordinates and the equinoctial orbital elements diverges when the interval time is more than 3 and 4 orbital periods, respectively.

Figure 5 shows the computation time of each filter, which is normalized by the value for the EnGMF with Cartesian coordinates. Compared to the AEGIS, the EnGMF reduces the computation time by 59.91% on average.

A more in-depth comparison of the performances of the EnGMF and AEGIS algorithms is shown for the ten-orbits interval periods. Figures 6 and 7 present the time history of the RMS position errors, SNEES

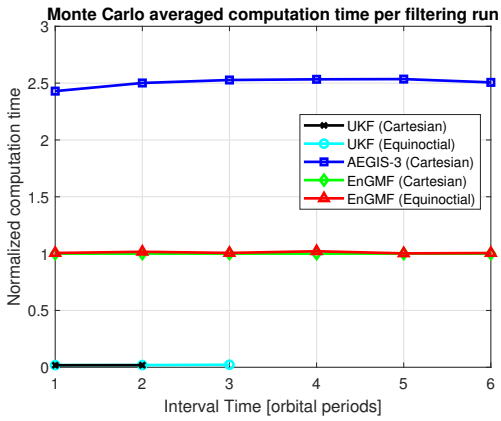

Figure 5. Monte Carlo averaged computation time per filtering run

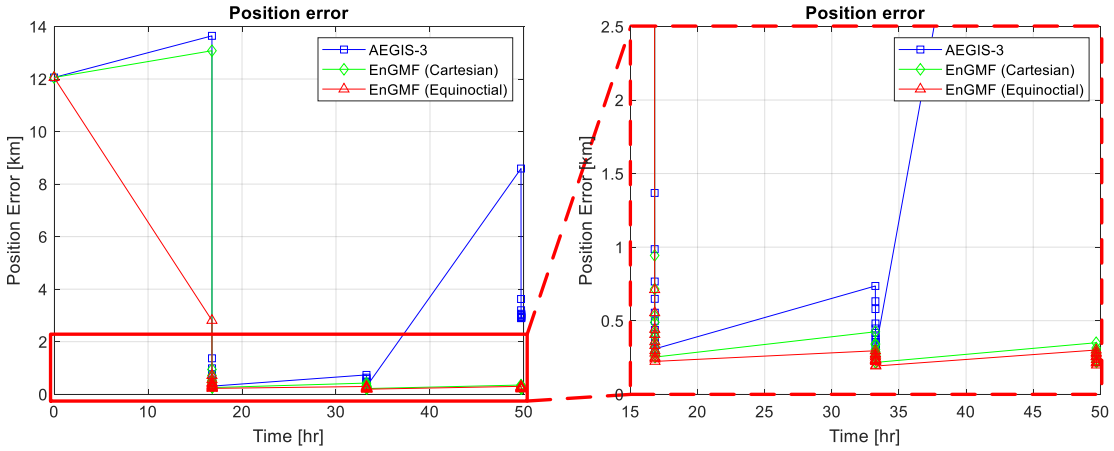

Figure 6. The average RMSE for 100 Monte Carlo simulations, the ten-orbits case

values, and average computation time per filtering run of the EnGMF and AEGIS, and each value is also described in Table 4. In terms of accuracy, the EnGMF with Cartesian coordinates or the equinoctial orbital elements outperforms the AEGIS method over time. This is because the AEGIS filter diverges in seven out of 100 simulations as shown in Figure 7(a), whereas the EnGMF is conservative. Moreover, Figure 7(b) shows that the EnGMF reduces the computation time by 60.57% compared to the AEGIS. In Table 4, we can see that the EnGMF using the equinoctial orbital elements obtains the best performance in terms of accuracy and mean computation time.

The performance of the estimators gets worse as the gap between measurement passes increases until it eventually diverges. To evaluate the performance of the EnGMF with the equinoctial elements under a sparser measurement data condition, a Monte Carlo analysis is performed with 100 simulations when the gap between measurement passes is increased to 20 orbital periods. The value of 20 orbital periods is chosen because it causes one divergence out of 100 runs when 1000 particles are used. The analysis is repeated for an EnGMF implementation with 2000 particles. Figures 8 and 9 show the time history of the RMS position errors, SNEES values, and average computation time of the 100 simulations, and each value is listed in Table 5. The result shows that the EnGMF with 2000 particles outperforms the EnGMF with 1000 particles in terms of the RMSE and SNEES, which is the result of EnGMF with 1000 particles diverging in one out of 100 Monte Carlo simulations as shown in Figure 9(a). The EnGMF with 2000 particles, however, requires

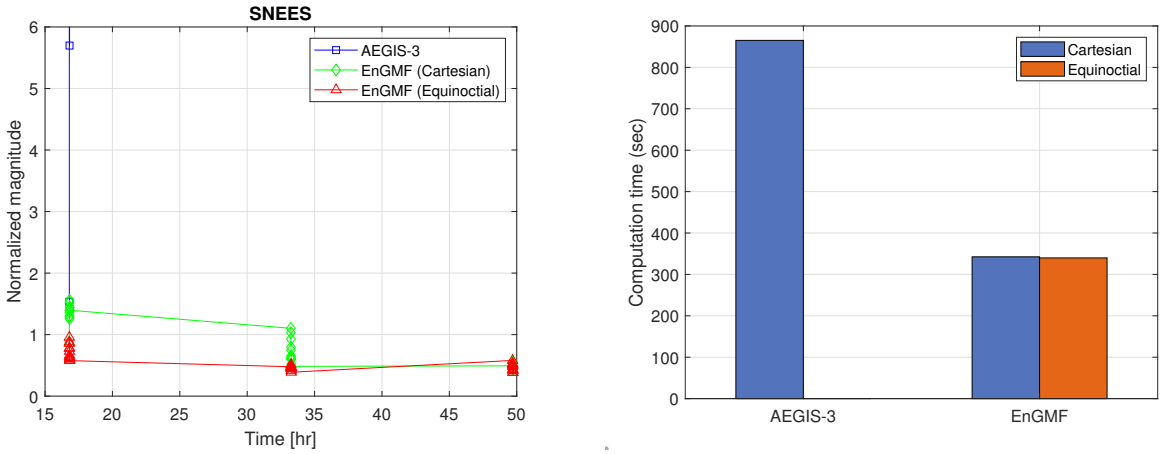

(a) The SNEES value

(b) The average computation time per filtering run

Figure 7. The SNEES value and the average computation time per filtering run for 100 Monte Carlo simulations, the ten-orbits case

Table 4. Monte Carlo averaged RMSE, SNEES, and computation time for the ten-orbits case

	Position's RMSE (km)	SNEES	Computation time (sec)
AEGIS-3 (Cartesian)	2.1578	1.6459e+06	865.17
EnGMF (Cartesian)	0.9930	0.8595	342.46
EnGMF (Equinoctial)	0.6688	0.5504	339.86

almost twice the computation time of the EnGMF with 1000 particles. Thus, the choice of the number of particles in the EnGMF is a trade between speed and accuracy/consistency. In other words, even if only a few observation data are available, the EnGMF with a large number of particles can provide accurate and consistent performance tracking SOs in LEO. In future work, we will investigate how to adaptively select an appropriate number of particles for very sparse measurement scenarios.

CONCLUSIONS

This paper studies a software-only solution to the orbit determination problem with sparse observation data. The motivation behind the study is the ability to maintain custody of a very large number of LEO objects. As such, it is of outmost importance in this study to strike a balance between estimation accuracy/consistency and computational burden of the methodology employed. A linear filter implementation (unscented Kalman filter) is shown to be inadequate for very scarce measurement scenarios (measurement passes every three orbits or more) regardless of the choice of coordinates (Cartesian or equinoctial orbital elements). A state-of-the-art Gaussian sum filter named AEGIS is shown to perform well at a very high computational cost, but to fail when the number of Gaussian components is artificially capped in order to

Table 5. Monte Carlo averaged RMSE, SNEES, and computation time for the twenty-orbits case

	Position's RMSE (km)	SNEES	Computation time (sec)
EnGMF-1000 (Equinoctial)	1.1135	989.5970	676.75
EnGMF-2000 (Equinoctial)	0.9372	0.6234	1374.26

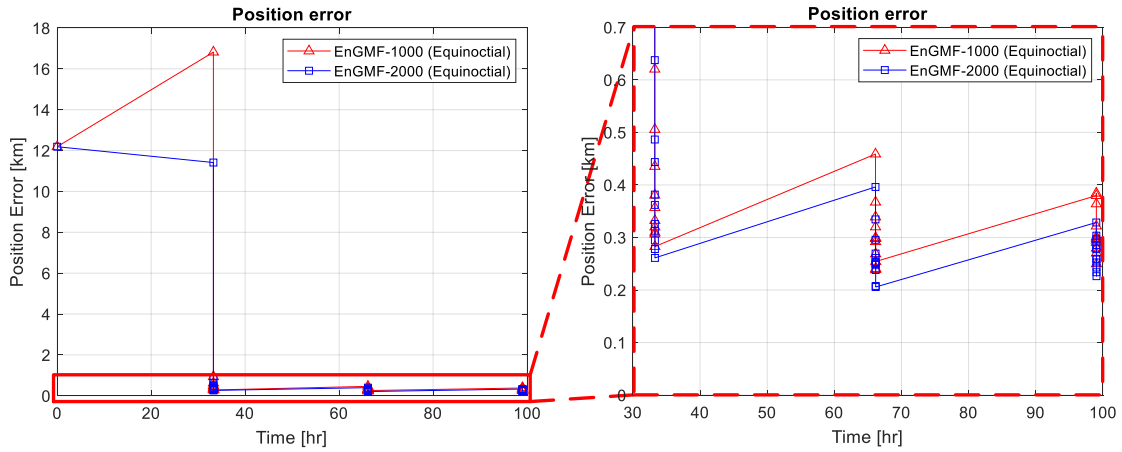

Figure 8. The average RMSE for 100 Monte Carlo simulations, the twenty-orbits case

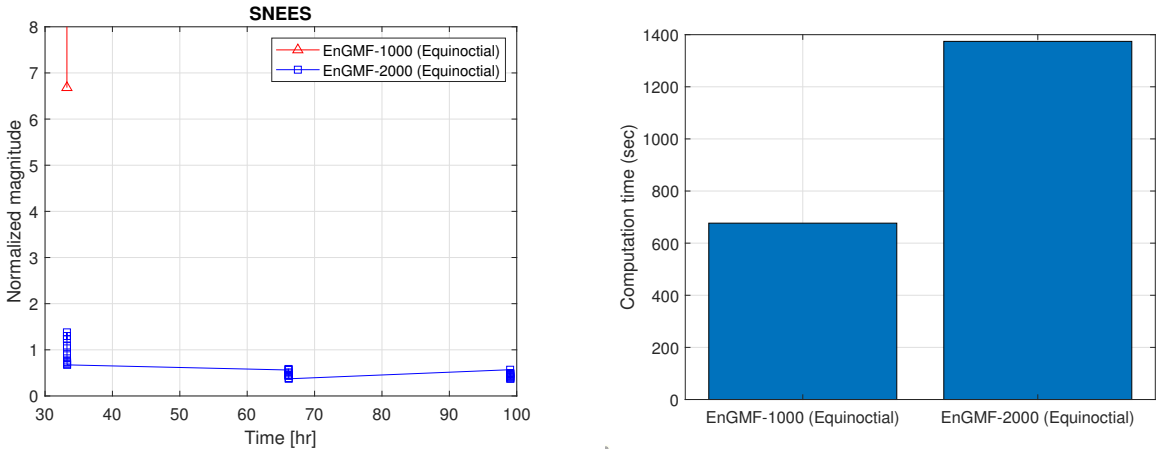

(a) The SNEES value

(b) The average computation time per filtering run

Figure 9. The SNEES value and the average computation time per filtering run for 100 Monte Carlo Simulations, the twenty-orbits case

contain its total execution time.

A newly proposed approach is to modify the kernel-based ensemble Gaussian mixture filter. Each propagated sample of the prior distribution is treated as a Gaussian component with a non-zero covariance matrix. The covariance matrix of a Gaussian component is calculated with Silverman's rule of thumb to reduce the computational cost of numerically optimizing a bandwidth parameter. The rule produces the optimal bandwidth when the samples are drawn from a Gaussian distribution, and results in a conservative estimate for non-Gaussian distributions. Numerical simulations show that the modified algorithm is more accurate and/or faster than the other approaches for sparse measurement scenarios. The conservatism inherent from using Silverman's rule cannot cause filter divergence but can result in slight loss of accuracy. This slight loss of accuracy is deemed an acceptable trade off to computational efficiency for the ultimate purpose of this work: tracking a very large number of space objects. While this conservatism can potentially trigger false collision alarms, an efficient strategy to maintaining a large catalog is using the proposed lower complexity and conservative estimates for the population at-large and to only focus high precision and computationally expensive orbit determination solutions for the very small subset of objects that are deemed at risk for

collision.

ACKNOWLEDGMENT

This work was sponsored in part by DARPA (Defense Advanced Research Projects Agency) under STTR contract number 140D0420C0062.

REFERENCES

[1] K. J. DeMars, M. K. Jah, and P. W. Schumacher, "Initial Orbit Determination using Short-Arc Angle and Angle Rate Data," *IEEE Transactions on Aerospace and Electronic Systems*, Vol. 48, No. 3, 2012, pp. 2628–2637. doi:10.1109/TAES.2012.6237613.

[2] E. Pate-Cornell and M. Sachon, "Risks of particle hits during space walks in low Earth orbit," *IEEE Transactions on Aerospace and Electronic Systems*, Vol. 37, No. 1, 2001, pp. 134–146. doi:10.1109/7.913673.

[3] T. Castaings, B. Pannetier, F. Muller, and M. Rombaut, "Track initiation in low-earth-orbit objects using statistical modeling of sparse observations," *IEEE Transactions on Aerospace and Electronic Systems*, Vol. 51, No. 1, 2015, pp. 258–269. doi:10.1109/TAES.2014.130484.

[4] National Research Council, *Continuing Kepler's Quest: Assessing Air Force Space Command's Astrodynamics Standards*. The National Academies Press, 2012.

[5] R. E. Kalman, "A New Approach to Linear Filtering and Prediction Problems," *Journal of Basic Engineering*, Vol. 82, March 1960, pp. 35–45. doi:10.1115/1.3662552.

[6] A. Gelb, ed., *Applied Optimal Estimation*. Cambridge, MA: The MIT press, 1974.

[7] S. J. Julier and J. K. Uhlmann, "Unscented filtering and nonlinear estimation," *Proceedings of the IEEE*, Vol. 92, March 2004, pp. 401–422. doi:10.1109/JPROC.2003.823141.

[8] K. J. DeMars, R. H. Bishop, and M. K. Jah, "Entropy-Based Approach for Uncertainty Propagation of Nonlinear Dynamical Systems," *Journal of Guidance, Control, and Dynamics*, Vol. 36, No. 4, 2013, pp. 1047–1057. doi:10.2514/1.58987.

[9] J. L. Anderson and S. L. Anderson, "A Monte Carlo Implementation of the Nonlinear Filtering Problem to Produce Ensemble Assimilations and Forecasts," *Monthly Weather Review*, Vol. 127, No. 12, 1999, pp. 2741–2758. doi:10.1175/1520-0493.

[10] R. A. Broucke and P. J. Cefola, "On the Equinoctial Orbit Elements," *Celestial Mechanics*, Vol. 5, No. 3, 1972, pp. 303–310. doi:10.1007/BF01228432.

[11] J. L. Junkins, M. R. Akella, and K. T. Alfriend, "Non-Gaussian Error Propagation in Orbital Mechanics," *Journal of the Astronautical Sciences*, Vol. 44, October - December 1996, pp. 541–563.

[12] C. Sabol, T. Sukut, K. Hill, K. T. Alfriend, B. Wright, Y. Li, and P. W. Schumacher, Jr., "Linearized Orbit Covariance Generation and Propagation Analysis Via Simple Monte Carlo Simulations," *20th Annual AAS/AIAA Space Flight Mechanics Meeting*, San Diego, California, February 15-17 2010.

[13] B. D. Tapley, B. E. Schutz, and G. H. Born, *Statistical Orbit Determination*. Elsevier Academic Press, 2004.

[14] P. J. Hughes and K. T. Alfriend, "Covariance Based Track Association with Modified Equinoctial Elements," *Proceedings of the 2020 AAS/AIAA Astrodynamics Specialist Conference*, 2020. Paper No. AAS 20-681.

[15] H. W. Sorenson and D. L. Alspach, "Recursive Bayesian Estimation Using Gaussian Sums," *Automatica*, Vol. 7, July 1971, pp. 465–479. doi:10.1016/0005-1098(71)90097-5.

[16] D. Alspach and H. Sorenson, "Nonlinear Bayesian estimation using Gaussian sum approximations," *IEEE Transactions on Automatic Control*, Vol. 17, August 1972, pp. 439–448. doi: 10.1109/SAP.1970.270017.

[17] J. T. Horwood and A. B. Poore, "Adaptive Gaussian Sum Filters for Space Surveillance," *IEEE Transactions on Automatic Control*, Vol. 56, No. 8, 2011, pp. 1777–1790. doi:10.1109/TAC.2011.2142610.

[18] J. T. Horwood, N. D. Aragon, and A. B. Poore, "Gaussian Sum Filters for Space Surveillance: Theory and Simulations," *Journal of Guidance, Control, and Dynamics*, Vol. 34, No. 6, 2012, pp. 1839–1851. doi:10.2514/1.53793.

[19] G. Terejanu, P. Singla, T. Singh, and P. D. Scott, "Adaptive Gaussian Sum Filter for Nonlinear Bayesian Estimation," *IEEE Transactions on Automatic Control*, Vol. 56, No. 9, 2011, pp. 2151–2156. doi:10.1109/TAC.2011.2141550.

[20] K. Tuggle and R. Zanetti, "Automated Splitting Gaussian Mixture Nonlinear Measurement Update," *Journal of Guidance, Control, and Dynamics*, Vol. 41, No. 3, 2018, pp. 725–734. doi:10.2514/1.G003109.

[21] S. Arulampalam, N. Gordon, and B. Ristic, *Beyond the Kalman Filter: Particle Filters for Tracking Applications Partical Filters for Tracking Applications*. Artech House, 2004.

[22] A. Doucet, N. de Freitas, and N. Gordon, *Sequential Monte Carlo Methods in Practice*. Information Science and Statistics, New York: Springer–Verlag, 2001.

[23] S. Yun and R. Zanetti, "Sequential Monte Carlo Filtering with Gaussian Mixture Sampling," *Journal of Guidance, Control, and Dynamics*, Vol. 42, No. 9, 2019, pp. 2069–2077. doi:10.2514/1.G004403.

[24] D. Raihan and S. Chakravorty, "Particle Gaussian mixture filters-I," *Automatica*, Vol. 98, 2018, pp. 331–340. doi:10.1016/j.automatica.2018.07.023.

[25] S. Yun and R. Zanetti, "Nonlinear filtering of light-curve data," *Advances in Space Research*, Vol. 66, No. 7, 2020, pp. 1672–1688. doi:10.1016/j.asr.2020.06.024.

[26] B. Liu, B. Ait-El-Fquih, and I. Hoteit, "Efficient Kernel-Based Ensemble Gaussian Mixture Filtering," *Monthly Weather Review*, Vol. 144, No. 2, 2016, pp. 781–800. doi:10.1175/MWR-D-14-00292.1.

[27] D. W. Scott, *Multivariate Density Estimation: Theory, Practice, and Visualization*. New Jersey, NJ: John Wiley and Sons, 1992. doi:10.1002/0470045345.

[28] B. U. Park and J. S. Marron, "Comparison of data-driven bandwidth selectors," *Journal of the American Statistical Association*, Vol. 85, No. 409, 1990, pp. 66–72. doi:10.1080/01621459.1990.10475307.

[29] M. C. Jones, J. S. Marron, and S. J. Sheather, "A brief survey of bandwidth selection for density estimation," *Journal of the American Statistical Association*, Vol. 91, No. 433, 1996, pp. 401–407. doi:10.2307/2291420.

[30] B. W. Silverman, *Density Estimation for Statistics and Data Analysis*. London: Chapman and Hall, 1986.

[31] N. K. Pavlis, S. A. Holmes, S. C. Kenyon, and J. K. Factor, "An Earth Gravitational Model to Degree 2160: EGM2008," *Proceedings of the European Geosciences Union General Assembly*, Vienna, Austria, April 13-18 2008.

[32] W. M. Folkner, J. G. Williams, D. H. Boggs, R. S. Park, and P. Kuchynka, "The Planetary and Lunar Ephemerides DE430 and DE431," IPN Progress Report 42-196, Jet Propulsion Laboratory, California Institute of Technology, http://ipnpr.jpl.nasa.gov/progress_report/42-196/196C.pdf, February 2009.

[33] D. A. Vallado, *Fundamentals of Astrodynamics and Applications, 3rd Edition*. New Jersey, NJ: McGraw-Hill, 1997.

[34] T. Lefebvre, H. Bruyninckx, and J. D. Schutter, "Comment on "A New Method for the Nonlinear Transformation of Means and Covariances in Filters and Estimators"," *IEEE Transactions on Automatic Control*, Vol. 47, No. 8, 2002, pp. 1406–1408. doi: 10.1109/TAC.2002.800742.

[35] E. A. Wan and R. V. D. Merwe, "The unscented Kalman filter for nonlinear estimation," *Proceedings of the IEEE 2000 Adaptive Systems for Signal Processing, Communications, and Control Symposium*, 2000. doi:10.1109/ASSPCC.2000.882463.

[36] M. Arulampalam, S. Maskell, N. Gordon, and T. Clapp, "A tutorial on particle filters for online nonlinear/non-Gaussian Bayesian tracking," *IEEE Transactions on Signal Processing*, Vol. 50, No. 2, 2002, pp. 174–188. doi:10.1109/78.978374.

[37] J. R. Dormand and R. J. Prince, "A family of embedded Runge-Kutta formulae," *Journal of Computational and Applied Mathematics*, Vol. 6, March 1980, pp. 19–26.

[38] Y. Bar-Shalom, X. R. Li, and T. Kirubarajan, *Estimation with Applications to Tracking and Navigation: Theory Algorithms and Software*. Wiley, 2001.

[39] R. Zanetti, K. J. DeMars, and R. H. Bishop, "Underweighting Nonlinear Measurements," *Journal of Guidance, Control, and Dynamics*, Vol. 33, No. 5, 2010, pp. 1670–1675. doi: 10.2514/1.50596.